

Materials Science | *Hot Paper* |


Bioinspired Scaffolding by Supramolecular Amines Allows the Formation of One- and Two-Dimensional Silica Superstructures

 Jose R. Magana, Berta Gumí-Audenis, Roderick P. Tas, Levena Gascoigne, Dylan L. Atkins, and Ilja K. Voets*^[a]

Abstract: Silica materials attract an increasing amount of interest in (fundamental) research, and find applications in, for example, sensing, catalysis, and drug delivery. As the properties of these (nano)materials not only depend on their chemistry but also their size, shape, and surface area, the controllable synthesis of silica is essential for tailoring the materials to specific applications. Advantageously, bioinspired routes for silica production are environmentally friendly and straightforward since the formation process is spontaneous and proceeds under mild conditions. These strategies mostly employ amine-bearing phosphorylated (bio)polymers. In this work, we expand this principle to supramolecular polymers based on the water-soluble cationic cyanine dye Pinacyanol acetate. Upon assembly in water, these dye molecules form large, polyaminated, supramolecular fibers. The surfaces of these fibers can be used as a scaffold for the condensation of silicic acid. Control over the ionic strength, dye concentration, and silicic acid saturation

yielded silica fibers with a diameter of 25 nm and a single, 4 nm pore. Unexpectedly, other unusual superstructures, namely, nummulites and spherulites, are also observed depending on the ionic strength and dye concentration. Transmission and scanning electron microscopy (TEM and SEM) showed that these superstructures are formed by aligned silica fibers. Close examination of the dye scaffold prior silicification using small-angle X-ray scattering (SAXS), and UV/Vis spectroscopy revealed minor influence of the ionic strength and dye concentration on the morphology of the supramolecular scaffold. Total internal reflection fluorescence (TIRF) during silicification unraveled that if the reaction is kept under static conditions, only silica fibers are obtained. Experiments performed on the dye scaffold and silica superstructures evidenced that the marked structural diversity originates from the arrangement of silica/dye fibers. Under these mild conditions, external force fields can profoundly influence the morphology of the produced silica.

Introduction


Rational design and controllable synthesis of silica (nano)materials are essential for developing and optimizing their applications. Scientific endeavors have focused on the development of synthetic routes to achieve nanometric control over silica structures. While solution-borne nucleation of silica precursors generally produces amorphous or spherical materials, condens-


ing silica on a supramolecular scaffold enables excellent control over the morphology (spheres, plates, cylinders), dimensions (nm to mm) and surface area.


Much of the research in this area is inspired by the bio-catalyzed and template-assisted formation of inorganic matter found in nature.^[1] Diatoms and sea sponges produce highly intricate silica structures with control over the morphology that is far greater than that achieved by humankind.^[2,3] Advantageously, biomineralization results in complex mesoporous silica architectures in a rapid and low-cost manner, since the formation process is spontaneous and catalyzed under mild conditions. Systematic studies to understand and mimic these natural processes have revealed that the silicic acid concentration, storage, and deposition rates are under strict biological control, assisted principally by amine-bearing phosphorylated (bio)polymers and membranes.^[4] These features modify the nucleation free energy barrier and nucleation kinetics of silica, which ultimately govern the growth into well-defined structures.^[5–10]

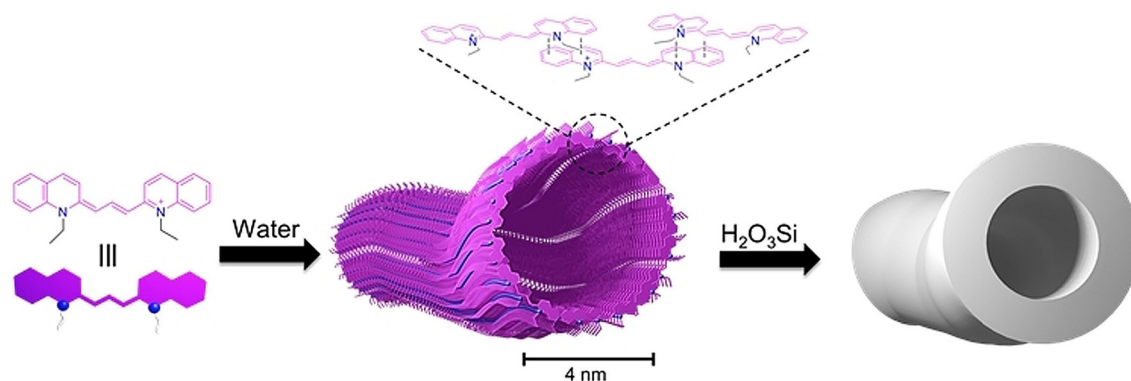
Building upon the lessons learned from insightful work on biomineralization, numerous silica production strategies have used amine-bearing polymers such as poly(ethyleneimine),^[11–13] polylysine,^[14–19] peptides,^[20–22] and block copolymers^[23–26] to obtain highly intricate structures. This method is advantageous

[a] Dr. J. R. Magana, Dr. B. Gumí-Audenis, Dr. R. P. Tas, L. Gascoigne, Dr. D. L. Atkins, Prof. I. K. Voets
 Laboratory of Self-Organizing Soft Matter
 Laboratory of Macromolecular and Organic Chemistry
 and Institute for Complex Molecular Systems
 Eindhoven University of Technology
 5600MB Eindhoven (The Netherlands)
 E-mail: i.voets@tue.nl

 Supporting information and the ORCID identification number(s) for the author(s) of this article can be found under:
<https://doi.org/10.1002/chem.202003139>.

 © 2020 The Authors. Published by Wiley-VCH GmbH. This is an open access article under the terms of Creative Commons Attribution NonCommercial-NoDerivs License, which permits use and distribution in any medium, provided the original work is properly cited, the use is non-commercial and no modifications or adaptations are made.

 Part of a Special Collection to commemorate young and emerging scientists. To view the complete collection, visit: [Young Chemists 2020](https://www.wiley.com/youngchemists).



Scheme 1. Schematic illustration of pinacyanol acetate (PIC) aggregates in aqueous solutions and their use as scaffolds for silicic acid condensation.

because the amine-rich polymers not only serve as a scaffold but also act as a catalyst to promote the condensation of silicic acid. In contrast to biomineralization processes, these strategies require the presence of solution-borne phosphate ions, which are thought to increase the condensation kinetics.^[9,27,28] Carefully tuning the chemical conditions, such as ionic strength and scaffold concentration, grants control over the morphology of the silica materials.^[4]

An impressive number of innovative routes to produce silica in a controlled manner has been developed using a handful of bio(macro)molecular analogs.^[13] Synthetic, supramolecular systems represent an appealing and as yet sparsely explored alternative for polyamine-mediated silica condensation. Supramolecular tectons amenable to amination and programmable self-assembly in aqueous media are abundant. Upon assembly, these can yield large, polyaminated, supramolecular surfaces for the condensation of silicic acid with a chemical composition, morphology, and dimensions that are tunable with external cues and/or by mixing of different interacting moieties. Understanding the factors that govern the controlled condensation of silicic acid would grant a tuning handle for further design of silica superstructures. An interesting class of fairly water-soluble, self-assembling molecules that fulfill these criteria are cyanine dyes, such as Pinacyanol acetate (PIC). These are flat aromatic dye molecules that self-assemble in water to produce hollow tubes or fibers (Scheme 1).^[29–31] Due to electrostatic repulsion, charged amines moieties are positioned to the outside of the tubes/fiber, where counterions predominantly reside. This yields a one-dimensional, supramolecular polyamine reminiscent of the covalent polyamines which guide biomineralization processes in diatoms and sea sponges.

Aiming to unravel the bioinspired formation pathways to prepare well-defined, complex silica nanostructures under mild reaction conditions with supramolecular amines, we herein investigate the delicate interplay between various factors that impact this pathway complexity. We first identify experimental conditions that give rise to well-defined, intricate silica morphologies in a robust manner. Next, we rationalize how the template concentration, phosphate concentration, and flow influence the mechanism of silica condensation. Finally, we present a state diagram that summarizes our main findings and

offers a guideline to promote templated and circumvent amorphous materials.

Results and Discussion

First, we set out to explore under what conditions supramolecular amines can be used as a template to direct silica condensation at neutral pH and room temperature. We use a weak phosphate buffer (PB) to maintain a constant pH and promote the polyamine-mediated condensation of silica, which requires the presence of phosphate ions. Multivalent salts, however, can cause phase separation of oppositely charged (poly)electrolytes in solution due to bridging. Indeed, while samples with low phosphate contents remained homogeneous, precipitation of the Pinacyanol acetate (PIC) dye was observed in samples with PB contents larger than 5 mM.

Next, PIC solutions were made in PB ranging from 1 mM to 3 mM, and dye concentrations ranging from 1 to 5 mM were incubated with tetramethyl orthosilicate (TMOS) in a 1:10 dye-to-silicic acid ratio for 24 hours. Subsequently, samples were centrifuged, washed with ethanol, and the silica solids analyzed by scanning electron microscopy (SEM). No silica was

Prof. Dr. Ir. Ilja K. Voets studied Molecular Sciences at Wageningen University in Wageningen, the Netherlands. She performed her PhD research on complex coacervate core micelles assembled from oppositely charged copolymers at the same university, after which she moved to the Adolphe Merkle Institute in Fribourg, Switzerland for a postdoctoral research stay to investigate the phase behavior of concentrated protein mixtures. In 2011 she returned to the Netherlands to develop her own line of research in physical chemistry as a university lecturer at the Department of Chemical Engineering and Chemistry and the Institute for Complex Molecular Systems at TU/e. Here, she was appointed associate professor in 2015 and then full professor in the field of Self-Organizing Soft Matter in 2018. In her research on (biological) soft matter, Voets seeks to understand the simple design rules that orchestrate how complex functionalities emerge from hierarchical self-organisation processes and to translate these into rational design strategies for innovative functional materials.



formed in the absence of either phosphate or dye, suggesting/showing that both substances are essential. SEM images of the obtained precipitate revealed only a few fibers and a high content of amorphous material regardless of the dye concentration or PB content (Figure 1 & Figure S2). This indicates that the PIC nanotubes do not efficiently template silica condensation under these conditions since the majority of silica structures do not resemble the morphology of the original scaffold. We tentatively attribute this apparent lack of templating to the high saturation of the silicic acid. At high supersaturations, solution-borne nucleation competes with PIC-templated nucleation, such that silica precipitation proceeds through both pathways. As a result, a high proportion of amorphous material is generated.

To explore whether the growth of silica on the supramolecular template is favored at a reduced hydrolysis rate and concomitantly reduced silicic acid saturation, we repeated the experiments using tetraethyl orthosilicate (TEOS) instead of pre-hydrolyzed TMOS as silica precursor. TEOS is a water-immiscible and stable silica precursor, but we found that PIC solutions promoted its hydrolysis into silicic acid at the formed TEOS/aqueous interface. For these experiments we used strong mechanical stirring to increase the interface between TEOS and the aqueous solution. Interestingly, these results suggest that the gradual administration of silicic acid allows it to condensate on the surface of the supramolecular tubes in a controlled manner. Scanning and transmission electron microscopy (SEM & TEM) of these templated silica samples revealed fibers with a diameter of ca. 30 nm containing a single pore of about 4 nm, matching the cross-section of PIC aggregates (Figure 2A & B).

Unexpectedly, the reaction yielded different silica morphologies depending on the phosphate and dye content, ranging from the anticipated fiber-like architectures (Figure 2A & B) to more exotic flat, nummulate-like plates (Figure 2C & D) and spherulites (Figure 2E & F) at 2 mM, 1 mM, and 3 mM, PB respectively. Both superstructures were usually found in coexistence with silica fibers and their sizes ranged from hundreds of nanometers to microns (Figure S3 and S4). Closer inspection with TEM exposed that these superstructures are in fact formed by aligned one-dimensional fibers.

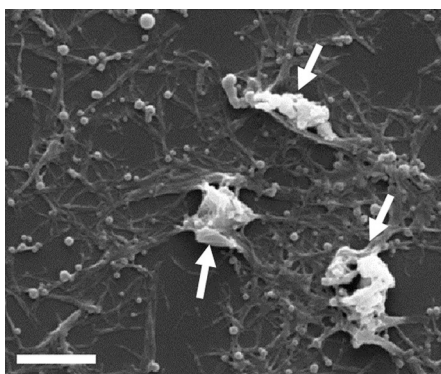


Figure 1. Scanning electron microscopy micrograph of silica nanostructures obtained at room temperature in 1 mM PIC and 5 mM PB using pre-hydrolyzed TMOS as a precursor. The arrows indicate the position of amorphous silica. The scale bar is 1000 nm.

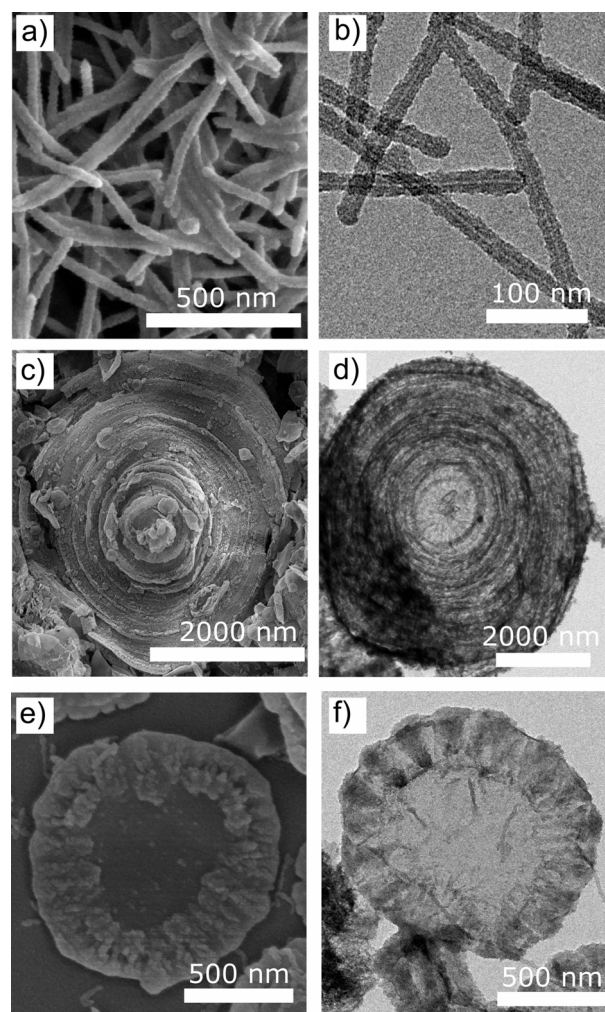


Figure 2. Electron microscopy observations of (A) SEM and (B) TEM of silica fibers prepared at 2 mM PB. (C) SEM and (D) TEM of nummulate structure prepared at 1 mM PB and (E) SEM and (F) TEM of silica spherulites made at 3 mM PB.

The above results clearly establish an impact of the amount of phosphate on the final structure. To elucidate whether this is due to an influence of the addition of ions on the aggregation behavior of PIC prior silicification, as observed for other charged dyes in solution,^[32] we first used UV/Vis spectroscopy (Figure 3). For this purpose, 0.1 mM PIC samples were prepared in PB with a phosphate ion concentration of 1 to 5 mM and in water (Figure 3). PIC shows metachromasia induced by the exciton delocalization into the dye aggregates. In the absence of phosphate ions, the PIC spectrum exhibits a low-intensity monomer vibronic band located at 600 nm and a high-intensity band and shoulder located at 545 nm and 525 nm, respectively.^[30–32] The latter are associated with the face-to-face H-aggregation state of PIC. Notably, upon addition of phosphate, the band at 545 nm is markedly reduced, while the band at 600 nm grows in intensity, and an extra red-shifted shoulder appears at 650 nm, suggesting that phosphate ions induce disassembly of aggregates and some dyes arrange into a head-to-tail fashion (J-aggregates).^[33] Further, an additional band ap-

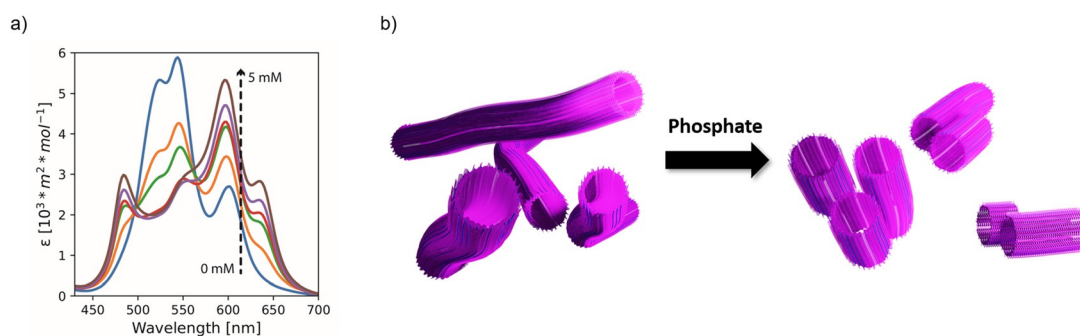


Figure 3. a) UV/Vis spectra of 0.1 mM PIC solution prior silicification in PB containing 0 mM, 1 mM, 2 mM, 3 mM, 4 mM and 5 mM phosphate ions. b) schematic representation of the influence of phosphate on the self-assembly properties of PIC.

peaks at 485 nm, which increased in intensity with phosphate concentration. This band is caused by strong electrostatic interaction between phosphate ions and the charged aggregate surface and is an indication of the formation of higher molecular weight supramolecular aggregates.^[32] Together, UV/Vis seems to indicate that although the dye fibers become smaller, the reduced electrostatic and phosphate bridging might bring the aggregates together to form bundles (Figure 3 b).

Whilst the aggregation tendency was clearly dependent on the phosphate ion concentration, small-angle X-ray scattering (SAXS) profiles of 10 mM PIC samples in (1 mM to 5 mM) PB prior silicification were very similar in the high- q regions at q -values $>0.1 \text{ \AA}^{-1}$. All displayed a characteristic oscillation for $0.1 \text{ \AA}^{-1} < q < 0.4 \text{ \AA}^{-1}$, indicating that the cross-section of the aggregates was virtually independent of phosphate content (Figure 4). Remarkably, no pronounced interference features were observed in the SAXS pattern for the PIC sample in water without phosphate ions. A modest increase in forward scatter-

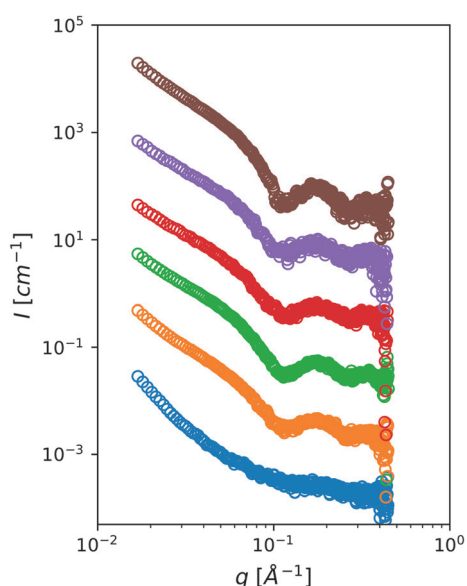


Figure 4. From bottom to top: small-angle X-ray scattering patterns of 10 mM PIC solutions at 0 mM, 1 mM, 2 mM, 3 mM, 4 mM and 5 mM phosphate prior silicification. For display purposes, the SAXS profiles are vertically shifted.

ing intensity with increasing phosphate ion concentration is noticeable at low- q values ($<0.1 \text{ \AA}^{-1}$). This signals that elevated phosphate contents give rise to attractive inter-aggregate interactions, which may induce hierarchical aggregation when the electrostatic repulsion between positively charged PIC aggregates is reduced sufficiently. A model of hollow fibers of ca. 4 nm in cross-sectional diameter and a wall thickness of 0.34 nm represents the experimental SAXS patterns well at $q > 0.1 \text{ \AA}^{-1}$ in good agreement with recent reports (see SI for more information on SAXS data interpretation).^[31] It is noteworthy that despite SAXS indicates little influence on the dye fiber morphology, from this results we cannot conclude that the fibers are not arranged already into nummulites or spherulites prior silicification, as the size of these superstructures might be outside of the resolution limit of the technique.

Contrasting with the marked influence of phosphate on the obtained silica structures, UV/Vis and SAXS revealed that phosphate had little impact on the fiber morphology of the dye aggregates. To better understand the origin of the distinct silica morphologies observed, we visualized the in situ interfacial condensation of silica using total internal reflection fluorescence (TIRF) microscopy (Figure 5 and supplemental movies). PIC is fluorescent in monomeric form with an emission maximum located at a wavelength $\lambda_{\text{em}} = 620 \text{ nm}$ ($\lambda_{\text{ex}} = 550 \text{ nm}$).^[30] In water, self-assembly-induced exciton delocalization quenches the fluorescence emission. Remarkably, when silicic acid condenses on the surface of PIC aggregates, PIC fluorescence is partially recovered. The reason for this behavior is not yet fully understood, but it is likely caused by partial disassembly of PIC aggregates into fluorescent monomers. It is conceivable that this is induced by the release of ethanol in the vicinity of the silica surface during TEOS hydrolysis. Strong, screened electrostatic attractions between the positively charged PIC nanotubes and silica nanostructures may also contribute. Regardless of its origin, the effect is exploited to monitor condensation events in situ by fluorescence microscopy. As expected, condensation occurred exclusively in the vicinity of the PIC/TEOS interface. Remarkably, only fibers were observed under TIRF regardless of the concentration of phosphate (1 mM to 5 mM) or dye (1 mM to 3 mM). At first sight, these findings appear at odds with the SEM and TEM results. However, the electron micrographs were obtained from samples that were under me-

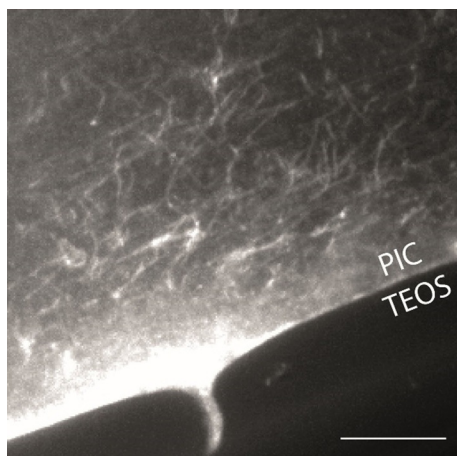


Figure 5. TIRF microscopy image of the interface between PIC and TEOS during silica condensation. The scale bar is 10 μm .

chanical stirring during the reaction, while TIRF microscopy was performed in situ under quiescent conditions. This suggests that the seemingly conflicting results may be explained by flow-induced alignment of silica fibers into hierarchical superstructures when silica is prepared under mechanical stirring. Moreover, TIRF and SAXS seem to indicate that the superstructures are indeed formed during mechanical stirring. Flow-induced arrangement of silica superstructures has already been reported in other biomineralization processes using the diatom-derived R5 peptide and polylysine. It is plausible that under these mild conditions and for slow kinetics of condensation compared to traditional sol-gel methods, external force fields can profoundly influence the morphology of the produced silica.^[10]

To validate this hypothesis, we once more prepared silica nanostructures from TEOS in the presence of PIC, but this time under static conditions, without mechanical stirring. As anticipated, fibers are produced under all quiescent conditions stud-

ied, including PIC and phosphate concentrations that yield nummulites and spherulites underflow. Fibers had a cross-sectional diameter of ca. 30 nm and were several microns long (Figure 6a–e), similar to those obtained in samples prepared under mechanical stirring. At phosphate concentrations higher than 4 mM, multi-fiber ribbons were found to coexist with these fibers (Figure 6e). This is likely caused by the fusion of single fibers due to phosphate bridging at high ionic strength.

After having established the influence of phosphate concentration, PIC concentration, and flow on the morphology of the produced silica nanostructures, we can now establish a state diagram to summarize the main findings (Figure 7). Static quiescent conditions produce exclusively one-dimensional silica nanostructures at the PIC (1 mM to 3 mM) and phosphate (1 mM to 5 mM) concentration studied. Ribbons composed of several bundles of fibers are observed in addition to well-dispersed fibers at $c_{\text{pho}} > 4$ mM. Mechanical stirring markedly impacts the morphology of the produced silica nanostructures. At PIC and phosphate concentrations below 1.5 mM and 1 mM, respectively, the precipitated silica fibers are coiled into flat nummulitic plates (Figure 2C & D). Condensation of silicic acid at slightly higher phosphate and PIC content yields almost exclusively silica fibers (Figure 2A & B). At phosphate and dye contents of 2 mM and 1.5 mM, respectively, PIC directs the formation of flat silica spherulites (Figure 2E & F). Finally, only amorphous silica is found in samples with phosphate ion or PIC concentrations higher than 2 mM.

The marked structural diversity originates from the pathway complexity of silica condensation. The key factors herein are the probability of silica condensation in bulk vs. on the PIC template, the flow-induced alignment of the PIC template, and the rate of silica condensation relative to the formation kinetics of the hierarchical superstructures. PIC/silica nanotubes remain well-dispersed in the absence of flow except at elevated ionic strength, where they fuse together into ribbons. Mechanical stirring induces the formation of different superstructures at the same conditions. The resulting morphologies are mainly

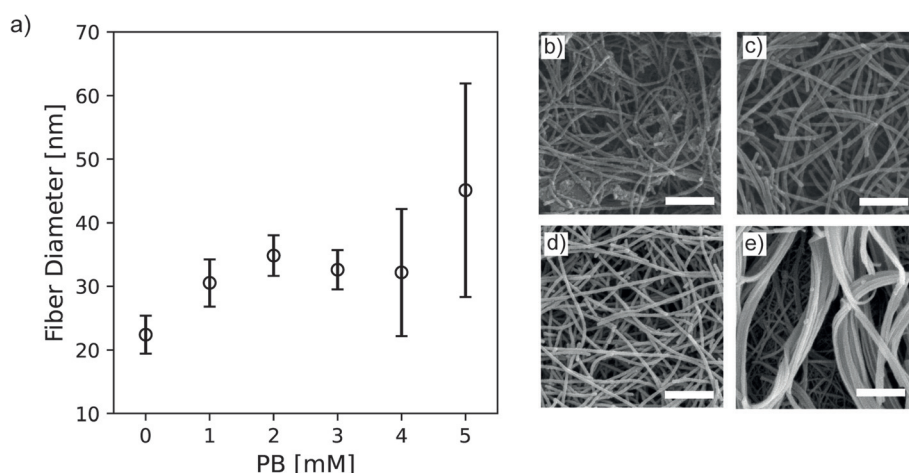


Figure 6. a) Cross-section thickness of silica fibers as a function of the phosphate content obtained at 20 °C and using 2 mM PIC at the non-disturbed TEOS-PIC interface. The inset images show SEM images of the silica fibers prepared in samples containing b) 1 mM, c) 2 mM, d) 3 mM, and e) 5 mM phosphate. Scale bar is 500 nm.

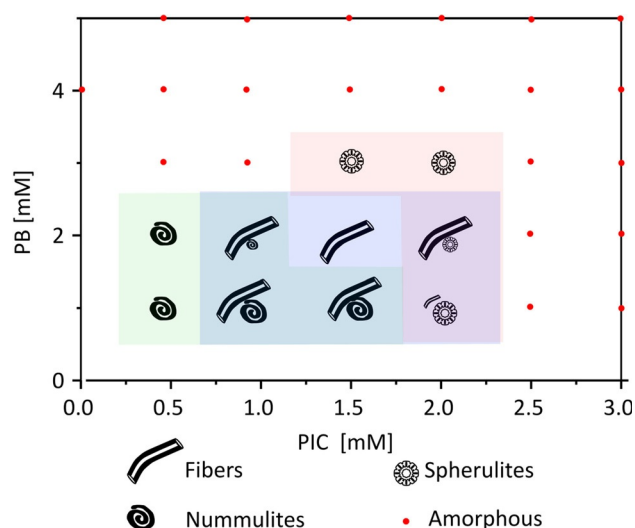


Figure 7. Morphology map showing the different silica nano-architectures as a function of PIC and phosphate concentration under mechanical stirring and at 20 °C. The size of the icons represents the relative abundance of each structure.

governed by nucleation kinetics. Under flow, an increase in PIC or phosphate concentration accelerates the rate of silica deposition. Low PB and PIC concentrations allow the controlled interaction of silica oligomers with dye aggregates and further alignment into nummulites before precipitating. With slightly higher phosphate content, silica nucleates faster, bypassing the alignment, and therefore, co-precipitating into single fibers. On the other hand, high PIC and phosphate concentrations promoted spherulites growth, which generally materializes in highly non-equilibrium systems. Possibly, silicic acid instantaneously condenses over the large surface area of the PIC fibers, which results in the formation of type II spherulites.

Finally, to elucidate what is the catalytically active species, monomeric and/or aggregated PIC, we induced PIC disassembly by increasing the ethanol volume fraction in the aqueous solvent. After 24 hours of reaction with TEOS under stirring at 20 °C, the precipitates were centrifuged and washed with ethanol, 1 M HCl, and water to remove phosphate ions that may interfere with further analysis. The dry solid was dissolved in concentrated NaOH, and the amount of silica was quantified by the molybdate blue assay (Figure 8). The yield of silica obtained after 24 hours remained constant up to 20% ethanol. Interestingly, the activity dropped at higher ethanol contents and was hindered already at 50% ethanol. The lack of activity at these conditions highlights the requirement of having a supramolecular arrangement of amines to promote silica formation. It would be interesting to examine in future work whether silica condensation activity is correlated with the silica surface area.

Conclusions

The supramolecular amine surface of PIC assemblies can promote and direct silica condensation into controlled morphologies from silicic acid at neutral pH and room temperature in

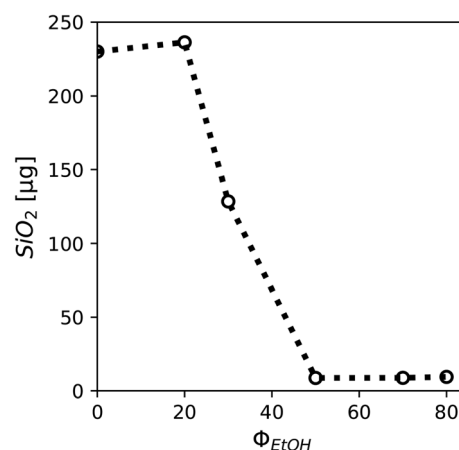


Figure 8. Amount of silica produced after 24 hours of reaction between TEOS and 1 mM PIC in 1 mM PB as a function of the ethanol volume fraction.

analogy to polyamines present in diatoms. Condensation kinetics and flow-induced alignment govern which silica morphology is produced. High silicic acid saturation levels lead to solution-borne nucleation and, consequently, inefficient templating. The silicic acid saturation level can be controlled by substituting prehydrolyzed TMOS for more stable TEOS. PIC solutions slowly hydrolyze TEOS into silicic acid, which is further condensed in a controlled manner on the supramolecular polyamine surface. SEM and TEM revealed that the templated silica fibers had a diameter of 25 nm containing a single pore of 4 nm, matching the cross-section of PIC aggregates. Unexpectedly, other unusual superstructures, reminiscent of nummulites and spherulites were additionally obtained, depending on the PIC and PB content.

UV/Vis and SAXS confirmed that the supramolecular PIC morphology prior silicification was nearly unaffected by phosphate ions. TIRF microscopy revealed that silica condensation into fibers occurred in the vicinity of the aqueous/TEOS interface. Seemingly in conflict with our first results, all conditions yielded silica fibers exclusively. This apparent contradiction was reconciled by the difference in flow conditions. Whilst fibers formed regardless of PIC and phosphate content at static and quiescent interfaces, exotic silica superstructures emerged in mixed bulk samples. Increments in either PIC or phosphate concentration, which accelerate silica deposition, afforded excellent control over the structure of the silica obtained. At low PIC and phosphate buffer concentration, silica fibers slowly grow and can further align into nummulites at the aqueous/TEOS interface. At slightly higher phosphate contents, silica condenses faster, impairing flow-alignment, thus producing single fibers. Instantaneous condensation of silicic acid on the high surface area of PIC aggregates results in the formation of spherulites. Finally, we demonstrated that the disassociation of PIC fibers inhibited silica condensation. These results highlight the extraordinary capacity of supramolecular amines to control the formation of silica superstructures at neutral pH and room temperature. Additionally, the morphology of the silica can be finely tuned by controlling the flow fields.

Acknowledgements

This work was supported by the Dutch Science Foundation (NWO VIDI Grant No. 723.014.006) and the Dutch Ministry of Education, Culture and Science (Gravity Program No. 024.001.035).

Conflict of interest

The authors declare no conflict of interest.

Keywords: materials science · mesoporous materials · nanotechnology · polyamines · superstructures

- [1] M. A. A. Abdelhamid, S. P. Pack, *Acta Biomater.* **2020**, <https://doi.org/10.1016/j.actbio.2020.05.017>.
- [2] M. B. Dickerson, K. H. Sandhage, R. R. Naik, *Chem. Rev.* **2008**, *108*, 4935–4978.
- [3] C. Sanchez, H. Arribart, M. M. G. Guille, *Nat. Mater.* **2005**, *4*, 277–288.
- [4] S. V. Patwardhan, S. J. Clarson, C. C. Perry, *Chem. Commun.* **2005**, *0*, 1113–1121.
- [5] F. Rodríguez, D. D. Glawe, R. R. Naik, K. P. Hallinan, M. O. Stone, *Biomacromolecules* **2004**, *5*, 261–265.
- [6] J. Yu, Q. Wang, X. Zhang, *Appl. Surf. Sci.* **2014**, *311*, 799–807.
- [7] R. Wu, Y. Li, Q. Wang, J. Yu, F. Jiang, F. Wang, X. Zhang, *RSC Adv.* **2012**, *2*, 9887–9893.
- [8] R. R. Naik, P. W. Whitlock, F. Rodriguez, L. L. Brott, D. D. Glawe, S. J. Clarson, M. O. Stone, *Chem. Commun.* **2003**, *9*, 238–239.
- [9] A. F. Wallace, J. J. DeYoreo, P. M. Dove, *J. Am. Chem. Soc.* **2009**, *131*, 5244–5250.
- [10] J. Zierenberg, P. Schierz, W. Janke, *Nat. Commun.* **2017**, *8*, 1–7.
- [11] N. Kröger, R. Deutzmann, C. Bergsdorf, M. Sumper, *Proc. Natl. Acad. Sci. USA* **2000**, *97*, 14133–8.
- [12] M. Sumper, E. Brunner, G. Lehmann, *FEBS Lett.* **2005**, *579*, 3765–3769.
- [13] V. V. Annenkov, E. N. Danilovtseva, V. A. Pal'shin, O. N. Verkhovzina, S. N. Zelinskiy, U. M. Krishnan, *RSC Adv.* **2017**, *7*, 20995–21027.
- [14] D. Noda, Y. Arai, D. Souma, H. Nagashima, R. H. Jin, *Chem. Commun.* **2014**, *50*, 10793–10796.
- [15] J. E. Baio, A. Zane, V. Jaeger, A. M. Roehrich, H. Lutz, J. Pfaendtner, G. P. Drobny, T. Weidner, *J. Am. Chem. Soc.* **2014**, *136*, 15134–15137.
- [16] L. Xia, B. Yao, H. Shi, Z. Shi, W. Wang, Z. Kan, *J. Sol-Gel Sci. Technol.* **2019**, *92*, 134–145.
- [17] J. Min, C. Ma, X. Liu, J. Li, H. Jiang, X. Wen, X. Chen, E. Mijowska, T. Tang, *ACS Omega* **2018**, *3*, 17573–17580.
- [18] Q. Wang, J. Yu, Y. Yan, S. Xu, F. Wang, Q. Li, J. Wang, X. Zhang, D. Liu, *Polym. Chem.* **2012**, *3*, 1284–1290.
- [19] S. V. Patwardhan, R. Maheshwari, N. Mukherjee, K. L. Kiick, S. J. Clarson, *Biomacromolecules* **2006**, *7*, 491–497.
- [20] B. Liu, Y. Cao, Z. Huang, Y. Duan, S. Che, *Adv. Mater.* **2015**, *27*, 479–497.
- [21] V. M. Yuwono, J. D. Hartgerink, *Langmuir* **2007**, *23*, 5033–5038.
- [22] Q. Wang, J. Yu, J. Zheng, D. Liu, F. Jiang, X. Zhang, W. Li, *RSC Adv.* **2013**, *3*, 15955–15965.
- [23] A. Sugawara-Narutaki, S. Tsuboike, Y. Oda, A. Shimojima, K. B. Landenberger, T. Okubo, S. Aoshima, *Langmuir* **2019**, *35*, 10846–10854.
- [24] G. Agrawal, S. K. Samal, S. K. Sethi, G. Manik, R. Agrawal, *Polymer* **2019**, *178*, 121599.
- [25] J.-S. Jan, D. F. Shantz, *Adv. Mater.* **2007**, *19*, 2951–2956.
- [26] J. N. Cha, G. D. Stucky, D. E. Morse, T. J. Deming, *Nature* **2000**, *403*, 289–292.
- [27] F. Daus, E. Pfeifer, K. Seipp, N. Hampp, A. Geyer, *Org. Biomol. Chem.* **2020**, *18*, 700–706.
- [28] K. G. Sprenger, A. Prakash, G. Drobny, J. Pfaendtner, *Langmuir* **2018**, *34*, 1199–1207.
- [29] J. R. Magana, M. Homs, C. Solans, M. Obiols-Rabasa, L. M. Salonen, C. Rodríguez-Abreu, *J. Phys. Chem. B* **2016**, *120*, 250–258.
- [30] C. Rodríguez-Abreu, C. A. Torres, G. J. T. Tiddy, *Langmuir* **2011**, *27*, 3067–3073.
- [31] J. R. Magana, C. Solans, L. M. Salonen, E. Carbó-Argibay, J. Gallo, G. J. T. Tiddy, C. Rodríguez-Abreu, *J. Taiwan Inst. Chem. Eng.* **2018**, *92*, 134–142.
- [32] R. C. Merrill, R. W. Spencer, B. R. C. Merrill, R. W. Spencer, *J. Am. Chem. Soc.* **1950**, *72*, 2894–2899.
- [33] S. Gadde, E. K. Batchelor, J. P. Weiss, Y. Ling, A. E. Kaifer, *J. Am. Chem. Soc.* **2008**, *130*, 17114–17119.

Manuscript received: July 1, 2020

Revised manuscript received: July 27, 2020

Accepted manuscript online: August 12, 2020

Version of record online: October 19, 2020